Enhanced and correlated thermal vibrations of Cu(111) and Ni(111) surfaces

T. Okazawa, F. Takeuchi, and Y. Kido*
Department of Physics, Ritsumeikan University, Kusatsu, Shiga-ken 525-8577, Japan
(Received 9 March 2005; revised manuscript received 2 May 2005; published 3 August 2005)

Enhanced and correlated thermal vibrations are studied for Cu(111) and Ni(111) by high-resolution medium energy ion scattering (MEIS) using the ion shadowing effect. We also perform molecular dynamics (MD) simulations based on the embedded atom method (EAM). The MEIS analysis reveals a slight contraction of 0.011 ± 0.003 and 0.007 ± 0.003 Å for Cu(111) and Ni(111), respectively, for the first interlayer distance without any surface reconstruction. The root mean square (rms) bulk thermal vibration amplitude and thermal vibration amplitudes (TVAs) of the top-layer atoms in the surface normal and lateral directions, respectively, are determined to be 0.085 ± 0.005, $0.141^{+0.010}_{-0.005}$, and $0.094^{+0.008}_{-0.005}$ Å for Cu(111) and 0.068 ± 0.005, $0.098^{+0.010}_{-0.005}$, and $0.074^{+0.008}_{-0.005}$ Å for Ni(111). We also observe strong correlations between the nearest-neighbor atoms in the [110] string and determine the correlation coefficients to be $+0.24 \pm 0.05$ and $+0.20 \pm 0.05$ for Cu(111) and Ni(111), respectively, for the motion perpendicular to the [110] axis. The present MEIS result is basically in agreement with the MD simulations using the EAM potential proposed by Foiles, Baske, and Daw [Phys. Rev. B **33**, 7983 (1986)] rather than that approximated by Oh and Johnson [J. Mater. Res. **3**, 471 (1988)].

DOI: 10.1103/PhysRevB.72.075408 PACS number(s): 68.35.Ja, 79.20.Rf, 63.90.+t

I. INTRODUCTION

High-resolution medium energy ion scattering (MEIS) spectroscopy provides a unique and powerful tool for determining precisely thermal lattice vibrations of bulk and surface together with correlations between neighboring atoms. Up to now, there are many reports on phonon dispersion relations along some high-symmetry directions in the first Brillouin zone (BZ) by neutron and light scattering in solids.[1–3] Electron energy loss spectroscopy and inelastic He-atom scattering determine the dispersions of surface phonons.[4–6] Of course, if the dispersion relations for a surface and bulk are completely known in the first BZ, one can deduce the thermal vibration amplitudes (TVAs) of the bulk and surface and also correlation coefficients between neighboring atoms. Thermal vibrations reduce diffraction intensity, known as the Debye-Waller factors. So far, surface Debye temperatures have been analyzed by low-energy electron diffraction (LEED) and reflection high-energy electron diffraction (RHEED).[7,8] Unfortunately, the above analyses cannot be made in a layer-by-layer fashion.

High-resolution MEIS allows a layer-by-layer analysis in near-surface regions and gives directly TVAs of bulk and surface atoms together with correlation coefficients between neighboring atoms. In previous works,[9–11] we analyzed the enhanced and correlated thermal vibrations for alkali halides and metal-oxides crystals. The results obtained by MEIS agree with those calculated by molecular dynamics (MD) simulations using appropriate pair potentials.[12] Up to now, there are a few reports on the enhanced and correlated thermal vibrations analyzed by MEIS.[13–16] However, the analytical treatments are incomplete and not systematic. In the present study, we further improved the depth resolution of MEIS and determined the TVAs of the bulk and surface atoms together with the correlation coefficient between the nearest-neighbor atoms for Cu(111) and Ni(111). The analysis technique employed here is different from those reported previously.[13–16] For comparison, the MD simulations were also performed based on the embedded atom methods (EAM).[17,18] One of the aims of this work is to evaluate the applicability of the EAM treatment to lattice dynamics of metal surfaces.

II. EXPERIMENT

The Cu(111) and Ni(111) clean surfaces were prepared by many cycles of sputtering with 1 keV Ar^+ and annealing at 620 °C for 2 to 10 min in ultra-high vacuum (UHV) and confirmed by RHEED, Auger electron spectroscopy, and MEIS. The annealing temperature was monitored with a Pt—Rh thermocouple. After confirming the 1×1 surface without any twins by RHEED, the sample was transferred into an UHV scattering chamber and mounted on a six-axis goniometer without exposure to air. All the analyses were made *in situ* under an UHV condition better than 2×10^{-10} Torr.

We employed 120 keV He^+ ions provided by a duoplasma ion source. The He^+ beam was collimated to a small size of 0.05 mm in the horizontal plane and 2.0 mm in the vertical plane. A toroidal electrostatic analyzer (ESA) detected the scattered He^+ ions with an excellent energy resolution ($\Delta E/E$) of 9×10^{-4}. The entrance slit size is 0.2 mm (horizontal) and 4.0 mm (vertical). The toroidal ESA has a wide interelectrode distance of 16 mm and a radius of 150 mm for the central circular trajectory in the horizontal plane. The ion-counting imager consists of a three-stage micro-channel plate combined with a position sensitive detector of a semiconductor type, which has a good position resolution of 40 μm. The detail was described in the literature.[19–22] In order to monitor the beam current precisely, the sample was biased by +90 V and the beam current was conducted to ground via an ammeter. To avoid radiation damage, we shifted the beam position slightly by 1 mm in the horizontal plane after an integrated beam current of 1 μC. Figure 1 shows a typical MEIS spectrum observed for

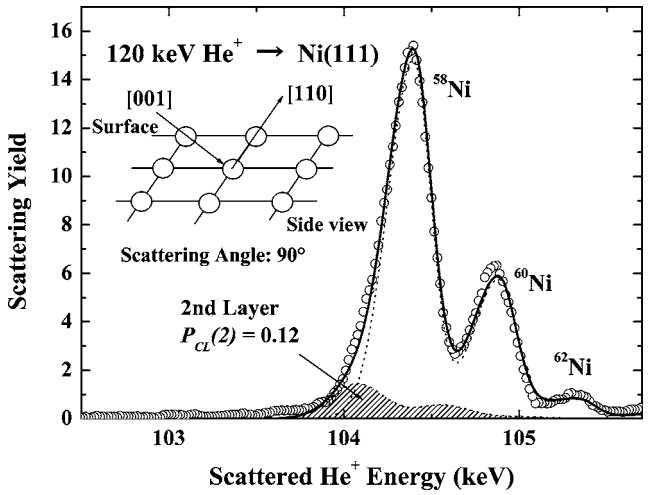

FIG. 1. MEIS spectra observed (open circles) and best-fitted (solid curve) for 120 keV He^+ ions incident along [001] axis of Ni(111) and scattered to [110] direction. The probability to hit the second layer Ni atoms ($P_{CL}(2)$) in the [001]-string is derived to be 0.12 by spectrum deconvolution (dotted curves) assuming asymmetric Gaussian shapes.

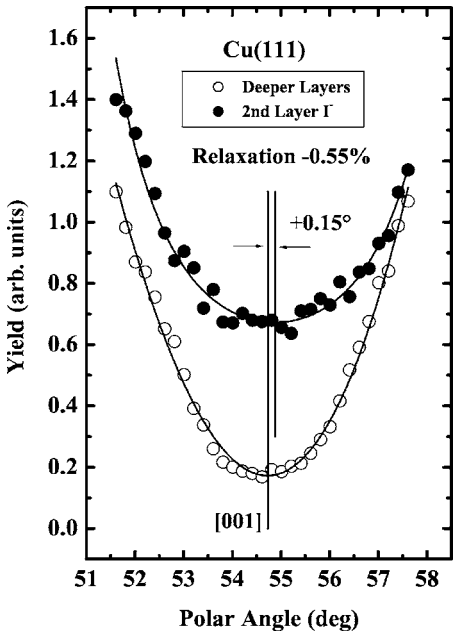

FIG. 2. Polar scan spectra observed for 120 keV He^+ ions incident around the Cu-[001] axis in the $(1\bar{1}0)$ plane. The open and full circles correspond to the scattering components mainly from the second-layer Cu atoms and from the deeper layers, respectively.

120 keV He^+ ions incident along the Ni-[001] axis and backscattered to the [110] direction. The solid curves are the best-fitted total and deconvoluted spectra with asymmetric Gaussian shapes. The best-fitting condition gives a hitting probability of 0.12 for the second-layer Ni atoms in the [001] string. Here, dividing the scattering yield from the nth-layer atoms by that from the top-layer atoms gives the hitting probability ($P_{CL}(n)$) for the nth layer atoms, which represents the extent of the ion shadowing effect quantitatively.

III. MD SIMULATIONS

MD simulations give not only a static surface structure but also dynamical characteristics such as lattice vibrations. In previous work,[9–11] we employed semi-classical pair potentials for alkali halide crystal surfaces. The results obtained by high-resolution MEIS are in good agreement with the MD simulations using the pair potentials proposed by Catlow *et al.*[12] It must be noted that simple pair potentials are applied to ionic crystals, in which the interactions between equivalent positive and negative point charges are essential. For metals, however, such a simple pair potential cannot be applied and more accurate treatments are required.

Based on the density functional theory,[23] the total electronic energy for an arbitrary atomic arrangement can be expressed by a unique functional of the total electron density. The idea of the EAM (Ref. 24) is to introduce the above density functional treatment and to approximate the electron density by the linear superposition of contributions from the individual atoms. Thus the total energy of a system is expressed in the form

$$E_{tot} = \sum_i F_i(\rho_{h,i}) + \frac{1}{2}\sum_i \sum_{j(\neq i)} \phi_{ij}(R_{ij}), \tag{1}$$

where $\rho_{h,i}$ is the host electron density at atom i due to the remaining atoms of the system and $F_i(\rho)$ is the energy gained by embedding atom i into the background electron density ρ. The second term in Eq. (1) represents the repulsive interaction potential between two positive cores, atom i and j separated by the distance R_{ij}. Here, it must be noted that F_i and ϕ_{ij} only depend on the element of atom i and on the elements of atoms i and j, respectively. As mentioned above, the total electron density is approximated by the superposition of the outer electron densities of the surrounding atoms,

$$\rho_{h,i} = \sum_{j(\neq i)} \rho_j(R_{ij}). \tag{2}$$

Such a treatment is reasonable for metals and alloys. The electron density for fcc transition metals is calculated from the Hartree-Fock wave functions[25,26] by

$$\rho(R) = n_s\rho_s(R) + n_d\rho_d(R). \tag{3}$$

Here, n_s and n_d are the number of outer s and d electrons and ρ_s and ρ_d are the electron densities associated with the s and d wave functions. Thus we calculate numerically the embedding function $F(\rho)$ for each element of metal and alloy. The effective charge in the core-core pair interaction ϕ_{ij} is also approximated by

$$Z(R) = Z_0(1 + \beta R^\nu)e^{-\alpha R}, \tag{4}$$

where Z_0 is the number of outer electrons and three parameters, α, β, and ν, are determined empirically to reproduce the elastic constant and vacancy formation energy. The force acting on the atom i is given by

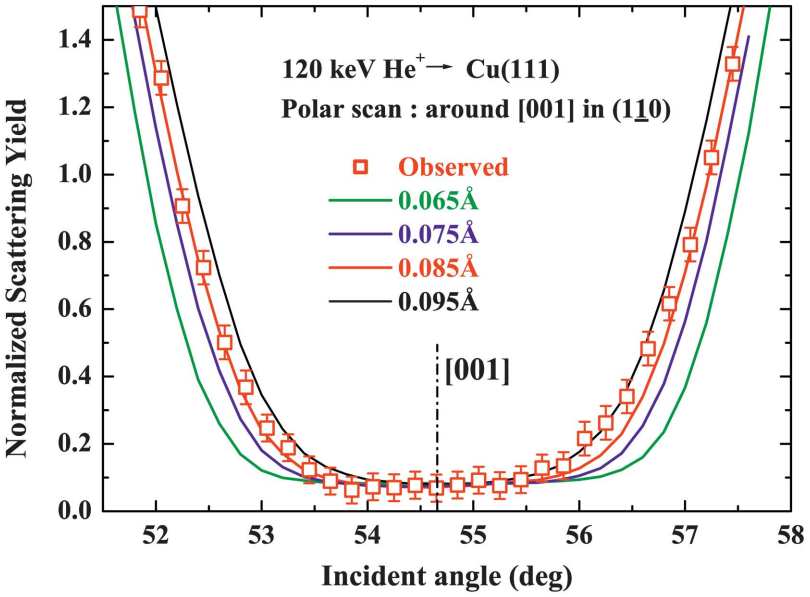

FIG. 3. (Color) Polar scan profile observed for He^+ ions incident around the Cu-[001] axis in the $(1\bar{1}0)$ plane for the scattering components mainly from the fifth to seventh layers. Four solid curves are calculated by Monte Carlo simulations of ion trajectories assuming the bulk TVA of 0.065, 0.075, 0.085, and 0.095 Å.

$$\vec{F}_i = -\nabla_i E_{tot}(\rho(R_i)). \tag{5}$$

Here, ∇_i means differentiation by $\vec{R}_i$ (position vector of atom i), namely $\Delta E_{tot}/\Delta \vec{R}_i$. The empirical parameters for Cu and Ni are given by Foiles, Baskes, and Daw,[17] as follows: Cu: $n_s=1$, $n_d=10$, and thus $Z_0=11$, $\alpha=1.7227$, $\beta=0.1609$, and $\nu=2$; Ni: $n_s=1.5166$, $n_d=8.4834$, and $Z_0=10$, $\alpha=1.8633$, $\beta=0.8957$, and $\nu=1$.

The numerical calculation based on the above treatment takes a long computing time. Oh and Johnson[18] approximated the above EAM expression and proposed a simple formula for the electronic energy for pure metals. The electron density ρ_i and the pair potential are approximated by

$$\rho_i = \sum_j f(R_{ij}), \quad f(R) = f_e \exp[-b(R/R_e - 1)],$$

$$\phi(R) = \phi_e \exp[-c(R/R_e - 1)], \tag{6}$$

where b, c, ϕ_e, and f_e are the empirical parameters given for each metal of interest and R and R_e are interatomic separation distance and its equilibrium value, respectively. The EAM function $F(\rho)$ is calculated numerically in advance. In these calculations, the f_e value plays no role for pure metals and is assumed to be unity. The empirical parameters and how to calculate $F(\rho)$ are referred to the literature.[18]

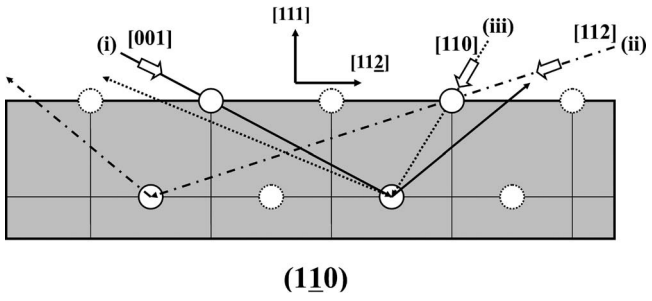

FIG. 4. Side view indicating three scattering geometries.

In the present MD simulations for Cu(111) and Ni(111), we set a basic cell consisting of 108 $(x,y)\times 18$ $(z)=2160$ atoms, which is surrounded by eight image cells placed in the (x,y) plane (x axis: $[1\bar{1}0]$, y axis: $[11\bar{2}]$). The equations of motion for all the atoms in the basic cell are solved numerically by the Verlet method at a time interval of 2.5 fs (10^{-15} s). The temperature was set to 300±5 K and the boundaries were fixed in the lateral plane (x,y) but not in the surface normal direction (z). A thermal equilibrium was confirmed by the velocity distribution coinciding exactly with the Maxwell distribution. The present cell size allows a minimum angular frequency down to $\sim 7\times 10^{12}$ rad s^{-1}. The contribution from the lower frequency is negligible, because the main contribution comes from 1.5 up to 4.5 $\times 10^{13}$ rad s^{-1} according to the density of state for Cu

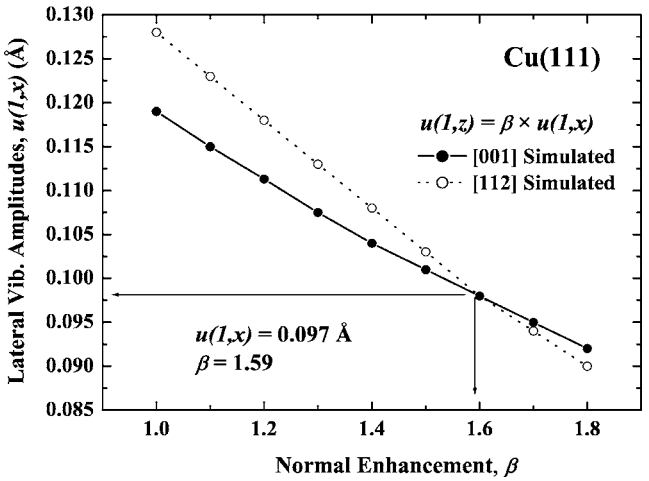

FIG. 5. Points $(u(1,x),\beta)$ satisfying the hitting probabilities $(P_{CL}^{001}(2)=0.45, P_{CL}^{111}(2)=0.30)$ for the second layer Cu atoms for [001] and $[11\bar{1}]$ incidence and random emergence. Here, β is defined by $u(1,z)\equiv\beta\cdot u(1,x)$. The crossing point $(u(1,x)=0.097$ Å, $\beta=1.59)$ gives just the real enhanced TVAs of the top layer Cu atoms.

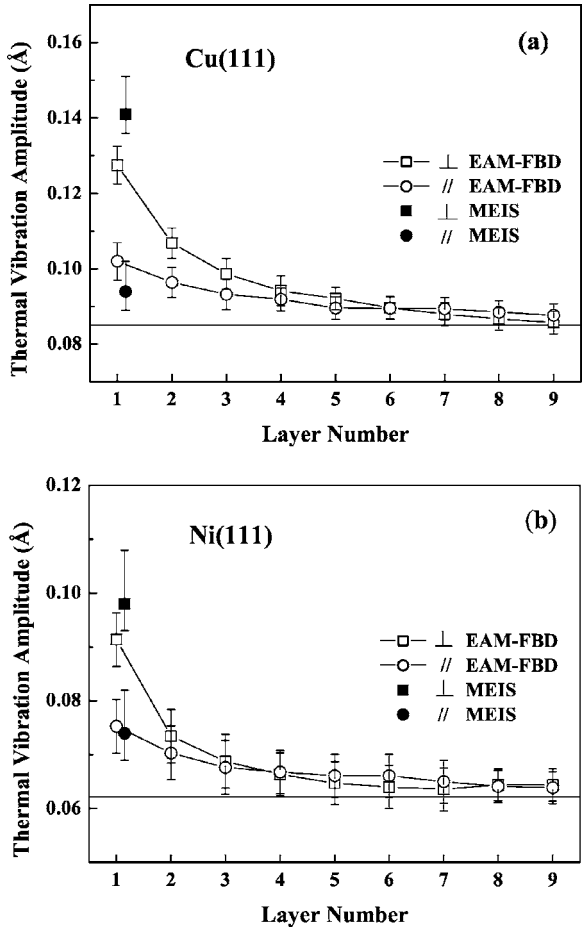

FIG. 6. Enhanced rms TVAs of the top layer atoms for (a) Cu(111) and (b) Ni(111). Open circles and squares denote the TVAs in the lateral (∥) and vertical (⊥) directions, respectively, for the top-down to ninth-layer atoms calculated from the MD (EAM-FBD). Full circle and square are the TVAs determined by MEIS in the lateral and vertical directions, respectively. The TVAs calculated from MD in the lateral direction are average values of those in the $x([1\bar{1}0])$ and $y([11\bar{2}])$ directions. (TVAs in the $[1\bar{1}0]$ direction are larger by about 10% than those in the $[11\bar{2}]$ for the top- and second-layer atoms.) The vertical lines attached to the symbols indicate experimental and statistical errors.

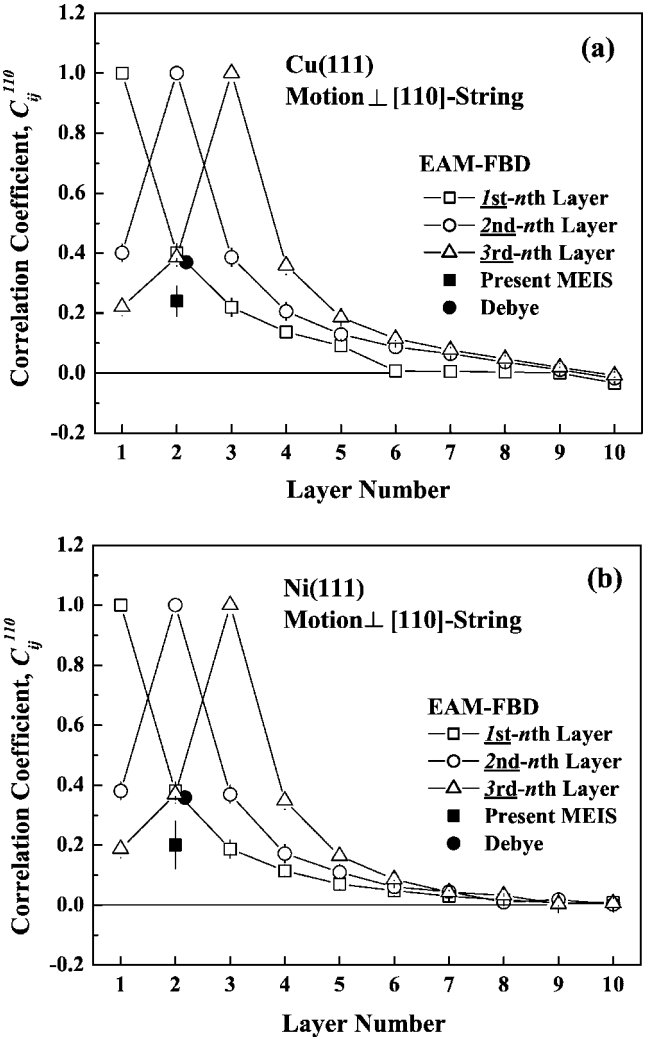

FIG. 7. Correlation coefficients calculated for (a) Cu(111) and (b) Ni(111) by the MD simulations (EAM-FBD) for neighboring atoms in the [110] string for the motion perpendicular to the [110]-axis. Open squares, circles, and triangles are the correlation coefficients for the top-, Second-, and Third-layer atoms with *n*th-layer atoms. The full squares and circles denote the present MEIS result and the Debye approximation, respectively.

observed by neutron scattering.[27] In the total energy calculations, we used the EAM expressions given by Foiles, Baskes, and Daw (EAM-FBD)[17] and Oh and Johnson (EAM-OJ).[18] The present MD simulations take account of the contributions from the first- and second-nearest-neighbor atoms only, because of very small contributions from the atoms farther apart.

IV. RESULTS AND DISCUSSIONS

First we determined the surface relaxation using the ion shadowing effect. Figure 2 shows the polar scan spectra for 120 keV He^+ ions around the Cu-[001] axis in the $(1\bar{1}0)$ plane. The open and full circles denote the scattering components mainly from the second-layer Cu atoms and from deeper layers below the fourth-layer, respectively. The angle giving the scattering yield minimum for the scattering component from the second layer slightly shifts by +0.15° from the [001] axis, indicating a small contraction of 0.011 ± 0.003 Å for the first interlayer distance between the top and second layers. The MD simulation based on the MD-FBD (Ref. 17) also gives a small contraction of 0.013 ± 0.005 Å, which is in good agreement with the present MEIS result. In contrast, the EAM-OJ (Ref. 18) predicts a considerably lager value of 0.079 Å. Such a small contraction of 0.01–0.02 Å was also observed by LEED (Ref. 28) and MEIS (Ref. 15) previously. In the case of Ni(111), the present MEIS analysis also revealed a small contraction of 0.007 ± 0.003 Å, which are compatible with the MD calculations of the EAM-FBD (0.003 Å) and the EAM-OJ (0.012 Å).

TABLE I. Surface relaxation, bulk, and enhanced TVAs, and correlation coefficients for nearest-neighbor atoms in the [110]-string for the motion perpendicular to the [110]-axis. The data obtained by present MEIS are compared with those calculated from the EAM-FBD[17] and EAM-OJ.[18]

	Relaxation Δd_{12} (Å)	Bulk TVA (Å)	$u(1,z)$ (Å)	$u(1,x)$ (Å)	$C_{12\text{-}[110]}$
Cu(111)					
Present MEIS	−0.011±0.003	0.085±0.005	$0.141^{+0.010}_{-0.005}$	$0.094^{+0.008}_{-0.005}$	+0.24±0.05
Previous MEIS (Ref. 15)	−0.026	0.078[a]	0.10	0.09	
EAM-FBD (Ref. 17)	−0.013±0.005	0.085±0.002	0.127±0.005	0.102±0.005	+0.38±0.03
EAM-OJ (Ref. 18)	−0.079±0.005	0.082±0.002	0.177±0.005	0.10±0.005	+0.63±0.05
Debye		0.084			+0.37
Ni(111)					
Present MEIS	−0.007±0.003	0.068±0.005	$0.098^{+0.010}_{-0.005}$	$0.074^{+0.008}_{-0.005}$	+0.20±0.05
EAM-FBD (Ref. 17)	−0.003±0.002	0.0621±0.002	0.0914±0.005	0.0753±0.005	+0.37±0.03
EAM-OJ (Ref. 18)	−0.012±0.005	0.0631±0.002	0.120±0.005	0.0705±0.005	+0.52±0.05
Debye		0.065			+0.359

[a]In Ref. 15, the bulk TVA derived from the Debye approximation at 0 K was assumed for Cu.

The bulk TVA can be derived by an angular scan around some major crystal axis for the scattering components from relatively deeper layers. Figure 3 shows the normalized scattering yield mainly from the fifth to seventh layers for 120 keV He^+ incidence as a function of polar angle around the Cu-[001] axis in the $(1\bar{1}0)$ plane. Four curves drawn are the polar scan profiles calculated from Monte Carlo simulations of ion trajectories assuming the bulk rms TVA (u_{bulk}) of 0.065, 0.075, 0.085, and 0.095 Å. Apparently, the assumption of 0.085 Å gives the best-fit to the observed polar scan profile. The present MEIS result coincides just with the value of 0.085±0.001 Å calculated from the EAM-FBD and also agrees with the value of 0.082±0.001 Å (EAM-OJ). If one assumes the Debye approximation, the bulk TVAs are deduced to be 0.077 and 0.084 Å for Debye temperatures (Θ_D) of 343 K (Refs. 29 and 30) and 315 K (Refs. 31 and 32), respectively. It must be noted that the former value was obtained by a calorimetric method at temperatures in the liquid helium range or lower and the latter was derived from heat capacity data at RT. The present MEIS data is in reasonably good agreement with the latter. For Ni(111), we also performed a polar scan around the Ni-[001] axis in the $(1\bar{1}0)$ plane and determined the u_{bulk} value to be 0.068±0.005 Å. This is compatible with that calculated from the EAM-FBD (0.062 Å), EAM-OJ (0.063 Å), and Debye approximations (0.065 Å, Θ_D=425 K).

Next we derive the enhanced TVAs of the top-layer atoms in the vertical and lateral directions and the correlation coefficient between the top- and second-layer atoms in the [110] string for the motion perpendicular to the [110] axis. For this purpose, the MEIS spectra were observed under the three different scattering geometries, as indicated in Fig. 4. Here, it is asssumed that the TVAs of atoms below the second layer are the same as those of the bulk and the correlations are neglected except for the nearest-neighbor atoms in the [110] string because of the smallest inter atomic distance (2.56 Å for Cu and 2.03 *Å* for Ni). We measured the MEIS spectra for (*i*) incidence along the [001] axis and backscattered to 80° (random direction) and for (*ii*) incidence along the $[11\bar{1}]$ axis and backscattered to 45° (random direction). The hitting probabilities for the second-layer Cu atoms are deduced to be 0.45 and 0.30, respectively, for the scattering geometries, (*i*) and (*ii*) by deconvoluting the surface peaks observed. Here, the observed surface peak is decomposed into three scattering components from the top, second, and third layers assuming an asymmetric Gaussian shape for each one. The existence of the stable isotopes [^{63}Cu(69%) and ^{65}Cu(31%), ^{58}Ni(68%), ^{60}Ni(26%), and ^{62}Ni(4%)] reduces the uncertainty of the deconvolution of the surface peaks. If the TVAs of the lattice site atoms are known, one can calculate the hitting probability for the atoms in each atomic layer by the Monte Carlo simulation of ion trajectories based on the binary collision approximation.[13] The fitting parameters to reproduce the observed hitting probabilities are the enhanced TVAs of the top-layer atoms in the lateral $[u(1,x)]$ and surface normal $[u(1,z)\equiv\beta\cdot u(1,x)]$ directions. Here, for simplicity, $u(1,x)=u(1,y)$ is assumed. Thus the combination of $(u(1,x),\beta)$ to reproduce the hitting probabilities observed for the two scattering geometries is drawn in Fig. 5. The crossing point for the two curves gives the actual values of 0.097 Å and 1.59 for $u(1,x)$ and β, respectively. As discussed below, the above analysis has an ambiguity concerning the significantly enhanced TVAs of the second-layer atoms [see Figs. 6(a) and 6(b)]. If one assumes the values of the enhanced TVAs derived from the MD simulations of EAM-FBD for the second-layer atoms, the TVAs for the top-layer atoms in the vertical and lateral directions are derived to be 0.141 and 0.094 Å, respectively. In quite the same manner, the $u(1,z)$ and $u(1,x)$ values for Ni(111) are determined to be $0.098^{+0.010}_{-0.005}$ and $0.074^{+0.008}_{-0.005}$ Å, respectively. The present MEIS result is consistent with the MD (EAM-FBD) predictions, as indicated in Figs. 6(a) and 6(b). The EAM calculations show that the TVAs decrease promptly with increase in the depth and become constant below the fourth-

layer but slightly larger than the bulk TVA. This is probably responsible for the size of the basic cell set in the present MD, in particular in depth.

Finally, we determine the correlation coefficient between the nearest neighbor atoms in the [110] string for the motion perpendicular to the [110] axis. The correlation coefficient, C_{ij} is defined by

$$C_{ij} = \frac{\langle u_i \cdot u_j \rangle}{\sqrt{\langle u_i \cdot u_i \rangle \langle u_j \cdot u_j \rangle}}, \tag{7}$$

where u_i means the displacement of an atom i from its equilibrium position and the bracket indicates a time average. The correlation between the top- and second-layer atoms in the [110] string was analyzed by the MEIS spectrum observed for (*iii*) [110] incidence and random emergence (see Fig. 4). If the TVAs of the top- and second-layer atoms and the correlation coefficient of interest are given, the hitting probability for the second-layer atoms is automatically decided. Here, it must be noted that the correlation for the motion parallel to the incident [110] axis does not contribute to the hitting probability. If one neglects the enhancement of the second-layer atoms, the correlation coefficient C_{12}^{110} is deduced to be $+0.24 \pm 0.05$. The assumption of enhanced TVAs of the second-layer atoms does not change the C_{12}^{110} value significantly, because it reduces the enhancement of the TVAs of the top layer atoms. In the case of Ni(111), the C_{12}^{110} value is derived to be $+0.20 \pm 0.08$. Such a strong positive correlation is quite reasonable, because of the acoustic phonon modes only. The present result is significantly lower than the calculated values from the EAM-FBD (+0.39 for Cu and +0.37 for Ni) and the Debye approximations (+0.37 for Cu and +0.359 for Ni) (see Fig. 7). This may be ascribed partly to some uncertainty in the deconvolution procedure. The extremely strong correlations predicted by the MD of EAM-OJ may be responsible for a small mismatch between the lattice constant set in the present MD and that giving a minimum total energy.

In Table I, the present MEIS result is compared with the EAM calculations and the MEIS data[15] reported previously. In the previous MEIS analysis,[15] the bulk TVA of 0.078 Å derived from the Debye approximation at 0 K was assumed and the enhanced thermal vibrations were estimated by fitting the simulated blocking profile to the observed one. It is seen that the present MEIS result is basically in agreement with the MD simulations based on the EAM-FBD model rather than the EAM-OJ. The bulk TVAs determined here agree well with the MD predictions from the EAM-FBD and EAM-OJ, and also from the Debye approximation. Concerning the correlation coefficient C_{12}^{110} for the nearest-neighbor atoms in the [110] string, the MEIS analysis gives significantly smaller values than those calculated from the MD simulations and Debye approximation. Neglect of the correlations for the atoms in the [001] and $[11\bar{1}]$ strings and some uncertainty in the deconvolution procedure may result in such inconsistency with the theoretical predictions.

V. SUMMARY

We analyzed the enhanced and correlated thermal vibrations for Cu(111) and Ni(111) by high-resolution MEIS. The results obtained are compared with the MD simulations using the EAM potentials proposed by Foiles, Baskes, and Daw (EAM-FBD) and by Oh and Johnson (EAM-OJ). It is found that the first interlayer distance for Cu(111) and Ni(111) is slightly shrunk within ~0.01 Å without any surface reconstruction. The MEIS spectra observed under various scattering geometries make it possible to deduce the TVAs of the bulk and top layer atoms in the vertical and lateral directions together with the correlation coefficient between the nearest neighbor atoms in the [110] string. The bulk and enhanced TVAs of the top-layer atoms determined here are compatible with the MD predictions based on the EAM-FBD and EAM-OJ. Concerning the correlation coefficient for the nearest-neighbor atoms in the [110] string, the MEIS analysis gives significantly smaller values than those calculated from the MD simulations and Debye approximation. Neglect of the correlations for the atoms in the [001] and $[11\bar{1}]$ strings and some uncertainty in the deconvolution procedure may result in such disagreement with the theoretical predictions. However, the present MEIS result is basically in agreement with the MD simulation of EAM-FBD rather than that of EAM-OJ. The EAM-FBD treatment could be widely applicable to surface structures and lattice dynamics of metals and also alloys.

ACKNOWLEDGMENTS

The authors would like to thank Professor S. Nakanishi and Dr. K. Umezawa for useful advice how to prepare the clean surfaces of Cu(111) and Ni(111). Special thanks are also due to their colleagues, Dr. T. Nishimura and Dr. Y. Hoshino, for assisting the MEIS experiments.

*Corresponding author. Electronic address: ykido@ritsumei.ac.jp

[1] E. C. Svensson, B. N. Brockhouse, and J. M. Rowe, Phys. Rev. **155**, 619 (1967).
[2] J. L. Warren, J. L. Yarnell, G. Dolling, and R. A. Cowley, Phys. Rev. **158**, 805 (1967).
[3] A. Mooradian, *Light Scattering Spectra of Solids*, edited by G. B. Wright (Springer, Berlin, 1969).
[4] C. Oshima, T. Aizawa, M. Wuttig, R. Souda, S. Otani, Y. Ishizawa, H. Ishida, and K. Terakura, Phys. Rev. B **36**, 7510 (1987).
[5] B. Voigtländer, S. Lehwald, H. Ibach, K. P. Bohnen, and K. M. Ho, Phys. Rev. B **40**, 8068 (1989).
[6] A. Lehmann, G. Fahsold, G. König, and K. H. Rieder, Surf. Sci. **369**, 289 (1996).
[7] U. Löffler, R. Döll, K. Heinz, and J. B. Pendry, Surf. Sci. **301**, 346 (1994).
[8] J. Vogt and H. Weiss, Surf. Sci. **501**, 203 (2002).
[9] T. Okazawa, T. Nishimura, and Y. Kido, Phys. Rev. B **66**, 125402

(2002).
[10] Y. Kido and T. Okazawa, Surf. Rev. Lett. **10**, 389 (2003).
[11] T. Okazawa, Y. Yagi, and Y. Kido, Phys. Rev. B **67**, 195406 (2003).
[12] C. R. A. Catlow, K. M. Diller, and M. J. Norgett, J. Phys. C **10**, 1395 (1977).
[13] J. F. van der Veen, Surf. Sci. Rep. **5**, 199 (1985).
[14] P. Statiris, H. C. Lu, and T. Gustafsson, Phys. Rev. Lett. **72**, 3574 (1994).
[15] K. H. Chae, H. C. Lu, and T. Gustafsson, Phys. Rev. B **54**, 14082 (1996).
[16] K. Kimura, K. Nakajima, and M. Mannami, Nucl. Instrum. Methods Phys. Res. B **136-138**, 1196 (1998).
[17] S. M. Foiles, M. I. Baskes, and M. S. Daw, Phys. Rev. B **33**, 7983 (1986).
[18] D. J. Oh and R. A. Johnson, J. Mater. Res. **3**, 471 (1988).
[19] Y. Kido, H. Namba, T. Nishimura, A. Ikeda, Y. Yan, and A. Yagishita, Nucl. Instrum. Methods Phys. Res. B **136–138**, 798 (1998).
[20] T. Nishimura, A. Ikeda, and Y. Kido, Rev. Sci. Instrum. **69**, 1671 (1998).
[21] Y. Kido, T. Nishimura, Y. Hoshino, and H. Namba, Nucl. Instrum. Methods Phys. Res. B **161–163**, 371 (2000).
[22] Y. Kido, S. Semba, and Y. Hoshino, Nucl. Instrum. Methods Phys. Res. B **219–220**, 559 (2004).
[23] W. Kohn and L. J. Sham, Phys. Rev. **140**, A1133 (1965).
[24] M. S. Daw and M. I. Baskes, Phys. Rev. Lett. **50**, 1285 (1983).
[25] E. Clementi and C. Roetti, At. Data Nucl. Data Tables **14**, 177 (1974).
[26] A. D. McLean and R. S. McLean, At. Data Nucl. Data Tables **26**, 197 (1981).
[27] S. K. Sinha, Phys. Rev. **143**, 422 (1966).
[28] S. Å. Lindgren, L. Walldén, J. Rundgren, and P. Westrin, Phys. Rev. B **29**, 576 (1984).
[29] *A.I.P. Handbook*, 3rd ed. (McGraw-Hill, New York, 1972).
[30] C. Kittel, *Introduction to Solid State Physics*, 3rd ed. (John Willey & Sons, New York, 1976).
[31] J. de Launy, in *Solid State Physics*, Vol. 2, edited by F. Seitz and D. Turnbull (Academic Press, New York, 1956).
[32] N. W. Ashcroft and N. D. Mermin, *Solid State Physics* (Harcourt Brace, New York, 1976).